MOLECULAR AND CELLULAR BIOLOGY, Aug. 2008, p. 4712–4718 Vol. 28, No. 15
0270-7306/08/$08.00+0 doi:10.1128/MCB.00237-08

The Headpiece Domain of Dematin Regulates Cell Shape, Motility, and Wound Healing by Modulating RhoA Activation[▽]

Morvarid Mohseni and Athar H. Chishti*

Department of Pharmacology, UIC Cancer Center, University of Illinois College of Medicine, Chicago, Illinois 60612

Received 12 February 2008/Returned for modification 31 March 2008/Accepted 19 May 2008

RhoA is known to participate in cytoskeletal remodeling events through several signaling pathways, yet the precise mechanism of its activation remains unknown. Here, we provide the first evidence that dematin functions upstream of RhoA and regulates its activation. Primary mouse embryonic fibroblasts were generated from a dematin headpiece domain null (HPKO) mouse, and the visualization of the actin morphology revealed a time-dependent defect in stress fiber formation, membrane protrusions, cell motility, and cell adhesion. Rescue experiments using RNA interference and transfection assays revealed that the observed phenotypes are due to a null effect and not a gain of function in the mutant fibroblasts. In vivo wounding of adult HPKO mouse skin showed a decrease in wound healing (reepithelialization and granulation) compared to the wild-type control. Biochemical analysis of the HPKO fibroblasts revealed a sustained hyperphosphorylation of focal adhesion kinase (FAK) at tyrosine 397 as well as a twofold increase in RhoA activation. Inhibition of both RhoA and FAK signaling using C3 toxin and FRNK (focal adhesion kinase nonrelated kinase), respectively, revealed that dematin acts upstream of RhoA. Together, these results unveil a new function of dematin as a negative regulator of the RhoA activation pathway with physiological implications for normal and pathogenic signaling pathways.

Dematin is an actin binding/bundling protein that was first isolated and characterized from the human erythrocyte membrane (16, 27). Purification of dematin from erythrocytes revealed a trimeric protein assembled by two polypeptides of 48 kDa and a 52-kDa polypeptide (15, 16). Each isoform consists of an actin binding headpiece domain at the C terminus and an N-terminal "core" domain (2). The headpiece domain is homologous to the headpieces of several proteins such as villin, a protein that is thought to be important for microvillus formation in the gastrointestinal tract (6, 23). The current model of the erythrocyte membrane places dematin at the junctional complex containing actin/spectrin and specifies that dematin is responsible for maintaining the shape and integrity of the erythrocyte (5, 7). Biochemical characterization of dematin has shown that it exhibits phosphorylation-dependent actin bundling activity (15, 16). The generation of the dematin headpiece knockout (HPKO) mouse permitted physiological evaluation of dematin's function in erythrocytes (17). The mutant mice exhibit mild spherocytosis and anemia, and the erythrocytes are osmotically fragile and mechanically unstable (17). Dematin is expressed predominantly in the hematopoietic (erythrocytes, platelets, and lymphocytes), cardiac, and vascular cells; brain; endothelial and epithelial cells; skeletal muscle; and kidney cells (1). The broad expression of dematin suggests that it may play a significant role in the regulation of the actin cytoskeleton in nonerythroid cells.

The overexpression of the core domain of dematin results in cytoplasmic shrinkage and extensive filopodial extensions, whereas overexpression of the headpiece domain results in lamellopodial and filopodial extensions (22). These defects suggest that dematin may play a conserved regulatory role in the cytoskeletal rearrangements. The most widely studied regulators of the actin cytoskeleton include the small family of Rho GTPases, Rac1, Cdc42, and RhoA, which cycle through an inactive GDP-bound state and an active GTP-bound state. RhoA has been extensively studied in a variety of biological processes including cell division, cell motility, and trafficking of receptors to the cell membrane (11). Activation of RhoA can be induced by a multitude of stimuli, including integrin-dependent cell adhesion and serum-dependent activation via the lysophosphatidic acid receptor (18). The downstream effector proteins of RhoA, the Rho-associated kinases and the nonkinase Rho effector protein mDia 1, directly regulate actin stress fiber formation (29). In addition to its effects on the actin cytoskeleton, RhoA also participates in the assembly of focal adhesions following cell-matrix interactions (4). It has been demonstrated, using the Rho-specific inhibitor C3 toxin, that RhoA signaling is involved in phosphorylation of focal adhesion kinase (FAK), a tyrosine kinase (18). In this study, we report a functional role for dematin in the regulation of cell shape and motility in nonerythroid cells derived from the dematin-expressing HPKO mice. Importantly, we provide the first evidence for a novel role of dematin as a suppressor of RhoA activation with physiological implications for the regulation of cytoskeletal arrangements in vivo.

MATERIALS AND METHODS

Cell culture, plasmids, and transfections. Mouse embryonic fibroblasts (MEFs) were isolated from HPKO and normal (wild-type [WT]) C57BL mice at embryonic day 13.5. Cells were cultured in Dulbecco's modified Eagle medium–10% fetal bovine serum for three passages prior to use. The cDNA for full-length dematin and the headpiece domain was subcloned into the pcDNA3-GFPmyc mammalian expression vector. Lipofectamine 2000 was used for transfection of cDNA constructs. A GTPase-linked immunosorbent assay kit for RhoA was purchased from Cytoskeleton Inc.

* Corresponding author. Mailing address: Department of Pharmacology, UIC Cancer Center, University of Illinois at Chicago, 909 South Wolcott Avenue, Room 5097, Chicago, IL 60612-3725. Phone: (312) 355-1293. Fax: (312) 355-1297. E-mail: chishti@uic.edu.

▽ Published ahead of print on 27 May 2008.

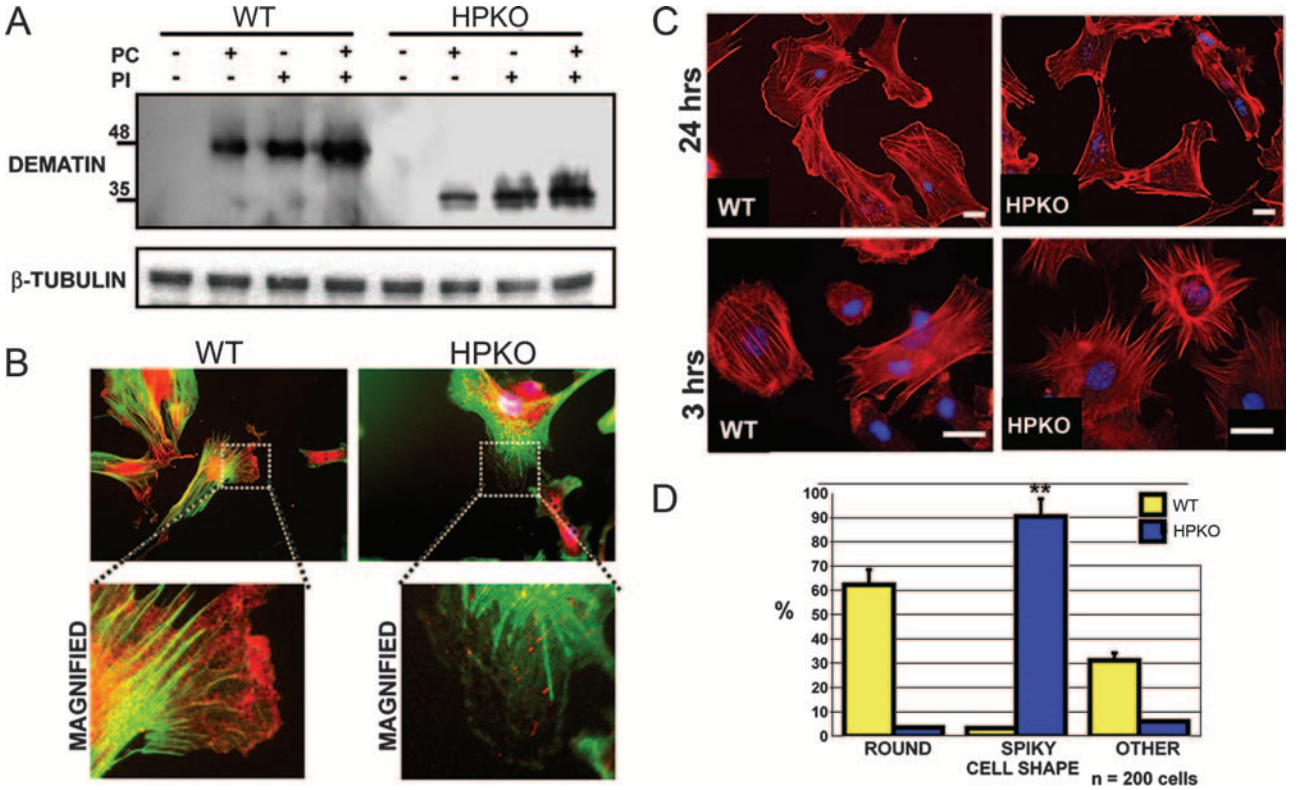

FIG. 1. Immunodetection of dematin and morphological defect in HPKO (KO) MEFs. (A) Western blot showing dematin expression in WT and HPKO MEFs treated with proteasome inhibitors (PI) MG132 and lactacystin and a protease inhibitor cocktail (PC). β-Tubulin was used as a loading control. (B) Immunofluorescence of WT and HPKO MEFs plated overnight. F-actin was visualized with phalloidin (green) and dematin (red) using a dematin monoclonal antibody. Magnification, ×20. The magnified bottom panels are at ×60. (C) WT and HPKO MEFs were stained for F-actin (red). WT and HPKO cells show no obvious phenotypic difference after 24 h of plating. Magnification, ×20; bar, 5 μm. In contrast, HPKO cells plated for 3 h and stained for F-actin show a marked phenotypic difference. Magnification, ×40; bar, 10 μm. (D) Quantification of cell morphology. MEFs were counted and grouped into "round," "spiky," and "other" categories.

Immunofluorescence and Western blotting. Monoclonal antibody against the core domain of human dematin was used (17). Alexa-conjugated antibodies were purchased from Molecular Probes. Monoclonal antibodies for FAK (A17) and polyclonal antibody pFAKY397 were from Santa Cruz, and monoclonal antibodies for Rac1, Cdc42, and RhoA were purchased from Cell BioLabs. β-Tubulin and β-actin monoclonal antibodies were purchased from Sigma. For detection of dematin by Western blotting, cells were treated with proteasome inhibitors lactacystin (10 μM) and MG-132 (5 μM) for 6 h. Cytosolic and membrane fractions were isolated by sonication of cells in lysis buffer (250 mM sucrose, 2 mM EDTA, 2 mM EGTA, 10 mM dithiothreitol, 1 mM phenylmethylsulfonyl fluoride, and a protease inhibitor cocktail). The lysate was centrifuged for 1 h at 45,000 rpm and 4°C. The supernatant containing the cytosolic fraction was removed. The remaining cell pellet was resuspended in lysis buffer containing 1% Triton X-100. The centrifugation was repeated, and the supernatant containing the membrane fraction was removed.

GTPase activation and adhesion assays. Analysis of Rac1, Cdc42, and RhoA activation was performed as previously described (3, 24). Inhibition of RhoA was performed by incubating cells in 7 μg/ml of cell-permeable C3 toxin (Cytoskeleton Inc.) for 3 h. Cells were also treated with 10 μM of Rho kinase inhibitor Y27632 (Calbiochem) for 1 h. Inhibition of FAK by FAK-related nonkinase (FRNK) was performed by Lipofectamine-based transfection of the cDNA construct of FRNK. Cell adhesion to fibronectin (FN) was measured using a crystal violet adhesion assay (13).

Motility and wound healing. For the in vitro wound healing assay, a confluent monolayer of cells was serum starved overnight and a scratch was introduced with a plastic pipette tip. Serum-containing media were reintroduced to the cells, and images of cell migration into the wound were captured until the wound was closed. Quantification of cell migration was done by measuring the distance between 10 random points within the wound edge. In vivo wound healing was performed on six mice from each genotype as described previously (10). Each mouse was anesthetized with 50 mg/kg of body weight of pentobarbital sodium (Nembutal), followed by six full-thickness dermal punch wounds (3 mm in diameter). At specific times after injury, mice were euthanized and the wounds were harvested for analysis. Each 3-mm wound was removed from the skin using a 5-mm-diameter punch. Individual wounds from each animal were processed by hematoxylin and eosin (HE) staining.

RNAi and real-time PCR. Two 25-mer stealth small interfering RNAs (siRNAs; RC1 and RC2) were designed through the Invitrogen RNA interference (RNAi) design algorithm, (RC1, 5′CCTCATCATGAATCCTCCAAGTT T3′; RC2, 5′TCCAACTTGGGAAAGATGATCTTGA3′). The siRNAs were optimal after 2 days of transfection at a 40 nM final concentration. Optimization and verification of dematin knockdown were performed using real-time PCR. Total RNA from RC1- and RC2-treated cells was collected with TRIzol (Invitrogen). Total RNA was converted to cDNA using oligo(dT) primers. cDNA (500 ng) was used for real-time PCR. Real-time PCR was performed using GAPDH (glyceraldehyde-3-phosphate dehydrogenase) and dematin primers and Applied Biosystems 2× Sybr green PCR master mix. The $\Delta\Delta C_T$ values (C_T, threshold cycle) and percent knockdown were quantified and normalized to those for GAPDH.

RESULTS

Dematin is expressed in MEFs. To examine the role of dematin in nonerythroid cells, a MEF primary cell line was generated from WT, C57, and HPKO mice. Since dematin contains a PEST motif (1, 25), immunodetection of dematin required the use of proteasome inhibitors MG-132 and lactacystin, as well as a protease inhibitor cocktail. Western blot

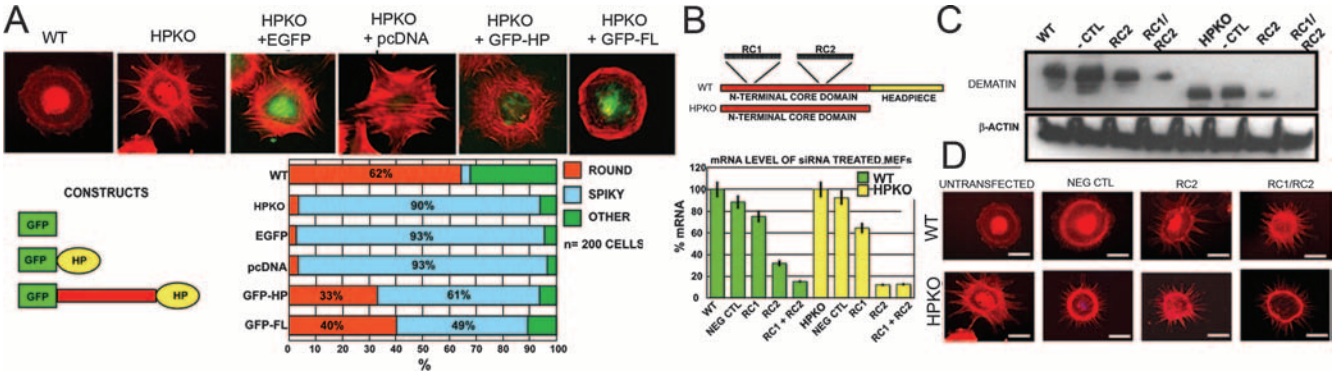

FIG. 2. Transfection-based rescue and RNAi-induced morphological defect. (A) Morphology rescue using dematin-green fluorescent protein (GFP) constructs transfected into HPKO (KO) MEFs. Magnification, ×40. (B) RNAi probes targeted to the core domain (RC1 and RC2) were used to knock down the expression of full-length (FL) dematin in WT cells and core domain expression in HPKO cells. Real-time PCR quantification of RNAi-induced knockdown of dematin in WT and KO MEFs is shown. (C) Western blot of dematin in siRNA-treated WT and HPKO MEFs. β-Actin was used as a loading control. (D) Actin morphology of siRNA-treated WT and HPKO MEFs plated for 3 h. Scrambled siRNA was used as a negative control (CTL). EGFP, enhanced GFP. Magnification, ×40.

analysis revealed a 48-kDa immunoreactive band in WT MEFs and a 37-kDa band in HPKO MEFs (Fig. 1A). The expression of truncated dematin in HPKO MEFs was ~50% less than that in WT MEFs. Immunolocalization of dematin in WT fibroblasts showed that dematin is located in the perinuclear compartment and in the cytosol, as well as in the membrane protrusions (Fig. 1B). In HPKO MEFs, truncated dematin is found in less abundance. It is not found in membrane protrusions; however, the truncated dematin is detectable in the perinuclear compartments of MEFs. Moreover, F-actin and dematin did not show a specific colocalization pattern, suggesting that dematin may not directly interact with F-actin in MEFs under these conditions.

HPKO MEFs show a morphology defect. To determine the effect of dematin mutation on cell shape changes, MEF morphology was assessed by F-actin staining with phalloidin (Fig. 1C). MEFs were plated and fixed over a time course of 24 h. After 3 h, WT MEFs show a rounded cell shape, whereas the HPKO MEFs exhibit a spiky morphology with a high frequency of membrane protrusions and stress fiber formation. After 24 h, the HPKO MEFs show an elongated morphology similar to that of the WT MEFs (Fig. 1C). Quantification of cell shape confirmed that the occurrence of the spiky phenotype in the HPKO fibroblasts is significantly higher than in the WT cells (Fig. 1D).

HPKO MEF morphology can be rescued. To determine if the HPKO phenotype is a direct consequence of the loss of dematin function, fibroblasts were transfected with specific dematin constructs (Fig. 2A). Fibroblasts were plated for 3 h and fixed and stained for F-actin (red). HPKO MEFs transfected with the enhanced green fluorescent protein and pcDNA3 vectors showed no change in morphology. HPKO fibroblasts transfected with the headpiece domain (HP) of dematin showed reduced occurrence of the spiky phenotype and an incomplete reversion to the WT cell morphology (Fig. 2A). Furthermore, HPKO fibroblasts transfected with the full-length 48-kDa isoform of dematin show a complete reversion back to the WT round cell phenotype. The WT cells exhibit two distinctive cell shapes: the more common round and the less common "elongated and spread" morphology, classified here as "other." In contrast, a significant percentage of HPKO cells show the spiky phenotype and less than 8% of HPKO cells show a round or "other" phenotype. Quantification of cell shape (n = 200 cells) revealed that ~40% of cells transiently transfected with the full-length dematin exhibit a WT round morphology (Fig. 2A).

The morphology defect is reproduced in siRNA-treated MEFs. To further verify the observed phenotypes, an RNAi approach was pursued. Two 25-mer stealth siRNAs (RC1 and RC2) that specifically target two sites within the core domain of dematin were generated (Fig. 2B). RC1 and RC2 were used separately (40 nM) and in combination (20 nM each) to specifically knock down the expression of dematin. A fluorophore-conjugated negative control siRNA was also used to determine any off-target effects, as well as the transfection efficiency, which approached ~75%. Quantitative real-time PCR determined the relative knockdowns of dematin in fibroblasts (Fig. 2B). WT and HPKO fibroblasts treated with RC1 attained 23% and 37% knockdown of dematin, respectively, whereas the RC2-treated WT and HPKO fibroblasts attained knockdowns of 70% and 90%, respectively. The fibroblasts treated with the combined RC1/RC2 showed substantial reductions: 85% in WT fibroblasts and 90% in the HPKO fibroblasts (Fig. 2B). Reduced protein expression was confirmed by Western blotting of cells treated with RC2 and RC1/RC2 using β-actin as a loading control (Fig. 2C). Due to the successful knockdown of dematin using RC2 and the combined RC1/RC2, these siRNAs were used for the morphology assays (Fig. 2D). MEFs treated with the negative control scrambled siRNA did not show any nonspecific effects. WT cells treated with RC2 and RC1/RC2 showed the spiky phenotype similar to that observed in the HPKO fibroblasts (Fig. 2D). It is noteworthy that, compared to fibroblasts with the genetic deletion of the dematin headpiece, the RC2- and RC1/RC2-treated fibroblasts appear to show a stronger phenotype with more-pronounced membrane protrusions. Since the untreated HPKO fibroblasts express the residual core domain, these experiments suggest that the core domain of dematin does not act in a gain-of-function manner.

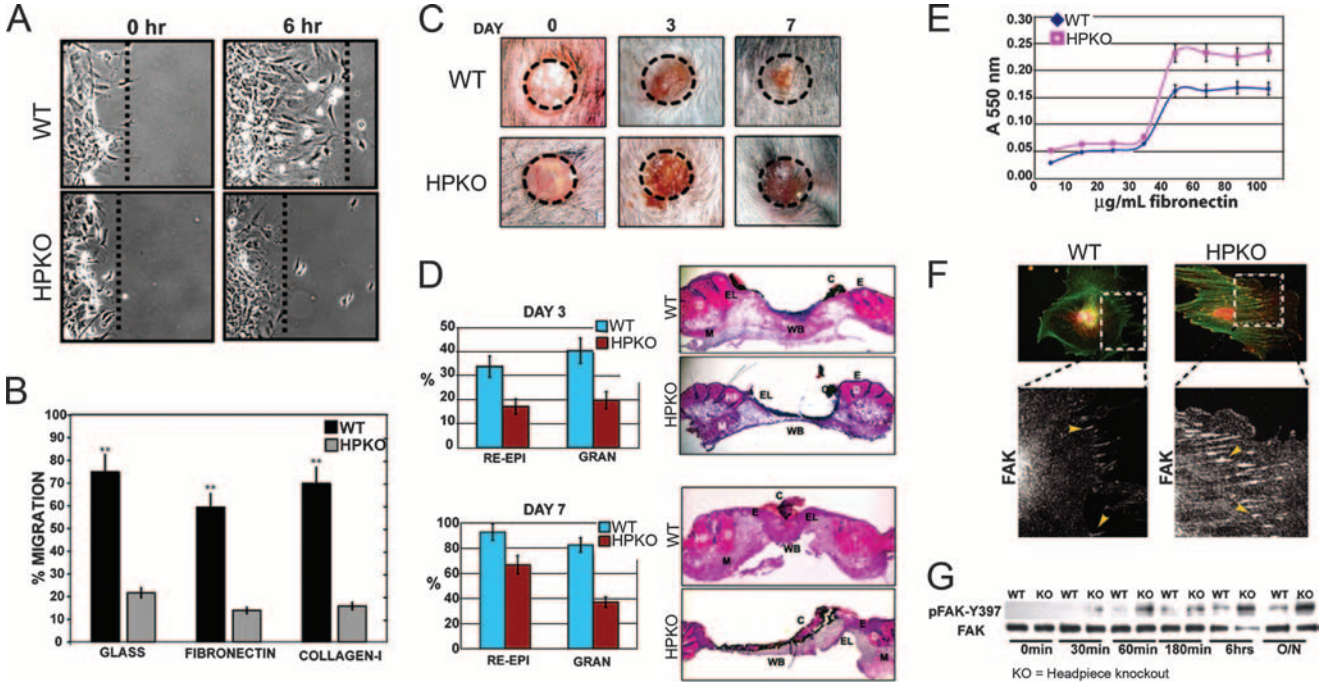

FIG. 3. Motility and adhesion defects in HPKO fibroblasts. (A) Scratch-induced motility assay of WT and HPKO (KO) MEFs. Dotted lines represent the wound edge. (B) Quantification of cell motility of WT and HPKO MEFs plated on glass, FN, and collagen-I. (C) Photographs of dermal wounds in WT and HPKO mice after 0, 3, and 7 days of wounding. (D) Quantification of wound reepithelialization (RE-EPI) and granulation (GRAN). HE staining of WT and HPKO wound sections after 3 and 7 days of wounding is shown. C, clot; E, epithelial layer; EL, epithelial lip; D, dermis; WB, wound bed; HF, hair follicle; M, skeletal muscle. (E) Crystal violet adhesion assay. (F) Immunofluorescence of F-actin (green) and focal adhesions using FAK-A17 (red) in WT and HPKO MEFs plated overnight. Magnification, ×20. The bottom panels show magnification of the above panels (magnification, ×60). (G) Western blot of WT and KO cells plated and analyzed for adhesion using FAK phosphorylated at Y397. O/N, overnight.

HPKO MEFs exhibit delayed cell migration. Fibroblast motility was assessed by a scratch-induced wound healing assay (Fig. 3A). WT and HPKO cells were serum starved overnight, and a scratch was introduced through confluent cells. Serum-containing media were reintroduced, and fibroblast migration was photographed until the wounds closed. The WT cells entered the wound space within 6 h; in contrast, the HPKO MEFs exhibit little motility, as visualized after 6 h. To quantify cell migration, cell motility was measured after 9 h of wounding. The WT cells migrated across ~73% of the wound in contrast to HPKO fibroblasts, which showed migration across ~20% of the wound (Fig. 3B). Moreover, transfection of the full-length dematin construct in HPKO cells partially rescued the cell migration phenotype (data reviewed but not shown). The relative motility defect remained unaltered irrespective of whether the cells were plated on FN or collagen-I, although the overall motility was somewhat reduced on both substrates (Fig. 3B).

Wound healing is impaired in HPKO mice. An in vivo wound healing assay was performed with WT and HPKO mice by generating six 3-mm wounds through the skin of each mouse. By day 3, WT wounds were moderately healed but, in the HPKO mice, the wounds appeared to show evidence of significant inflammation (Fig. 3C). By day 7, WT mouse wounds had almost completely healed, whereas HPKO mouse wounds were larger, showing significant inflammation (Fig. 3C). Tissues were harvested and sectioned from mice of both genotypes, followed by HE staining. The HE staining revealed that the HPKO mice show pronounced defects in fibroblast migration and granulation in the dermis, which were observed in tissues harvested from both day 3 and day 7 specimens (Fig. 3D).

Enhanced adhesion and FAK activation in HPKO fibroblasts. The adhesion of WT and HPKO fibroblasts to FN and collagen-I was determined using a crystal violet adhesion assay (Fig. 3E). With increasing concentrations of FN/collagen-I, the WT and HPKO cells adhered more, as represented by an increase in the absorbance. The HPKO cells show an ~1.5-fold increase in cell adhesion to FN (Fig. 3E), suggesting that the HPKO MEFs adhere better to the extracellular matrix than WT cells. To investigate this further, immunodetection of focal adhesion complexes was performed after plating the fibroblasts overnight. Upon adhesion to FN, larger and more-elongated focal adhesions are formed in the HPKO MEFs (Fig. 3F). Activation of FAK was determined by measuring its phosphorylation at tyrosine 397. The WT cell lysates show a weaker pFAKY397 band after 60 min of adhesion than HPKO cell lysates. FAK activation increased with time of adhesion of HPKO fibroblasts, showing an ~1.7-fold increase in FAK phosphorylation after overnight adhesion (Fig. 3G).

HPKO fibroblasts exhibit increased RhoA activation and membrane translocation. Rac1 and Cdc42 activation assays were performed using glutathione *S*-transferase (GST)–p21-activated kinase binding domain beads, and the RhoA activa-

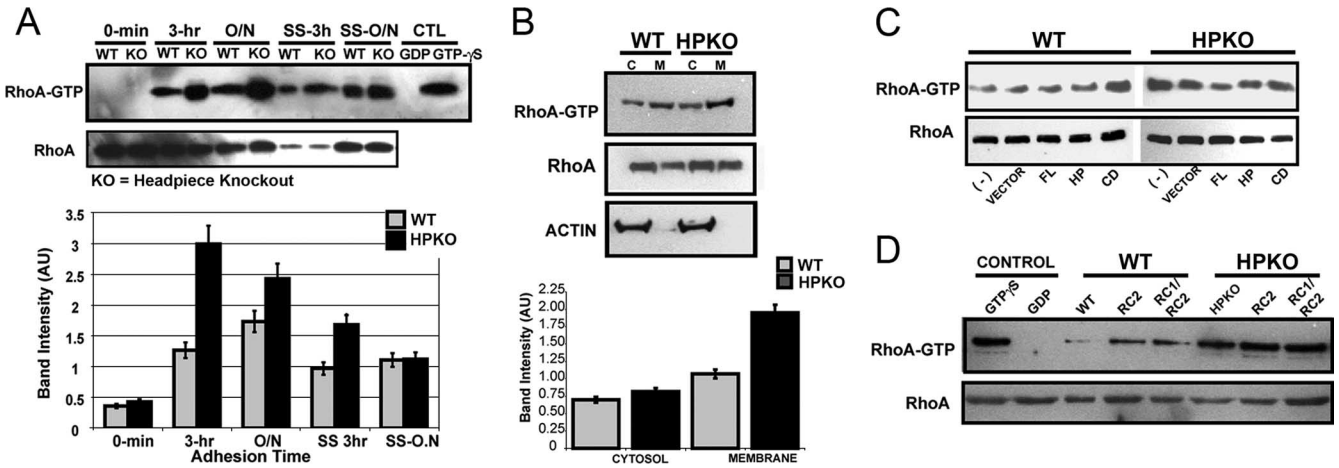

FIG. 4. Increased RhoA activation in HPKO fibroblasts. (A) GST-rhotekin-RBD pulldown assay using WT and HPKO (KO) cell lysates plated at several time points in serum-containing media or plated under serum-starved (SS) conditions. A representative blot of multiple experiments and quantification of RhoA activation in WT and HPKO cells are shown. O/N, overnight; CTL, control. (B) Cellular fractionation of WT and KO MEFs. A representative Western blot showing RhoA activation in the cytosolic (C) and membrane (M) fractions using a rhotekin-RBD pulldown assay and quantification of RhoA activation in the cytosolic and membrane fractions are shown. (C) Western blot of WT and HPKO cell lysates transfected with full-length (FL) dematin or the headpiece (HP) or core domain (CD) of dematin, followed by pulldown with rhotekin-RBD. (D) Rhotekin-RBD pulldown of dematin siRNA-treated WT and HPKO cell lysates.

tion assay was performed using GST-rhotekin-RhoA binding domain (RBD) beads. Lysates of MEFs plated at multiple time points revealed that Rac1 and Cdc42 activation is not altered in the HPKO fibroblasts (data not shown). In contrast, RhoA activation was significantly enhanced in HPKO fibroblasts, with the greatest difference observed during the initial phase of adhesion and spreading (30 min to 3 h) (Fig. 4A). Furthermore, phosphorylation of myosin light chain, a downstream effector of RhoA, was increased by ~45% at Thre-18 and Ser-19 residues, as determined by Western blotting, suggesting that the downstream signaling from RhoA is also perturbed in the HPKO fibroblasts (data not shown). To determine if the increased RhoA activation was due to an adhesion-dependent event or due to growth factor dependence, cells were serum deprived overnight and replated for 3 h. Under serum-free conditions, the HPKO fibroblasts continue to show an approximately twofold increase in RhoA activation at 30 min (data reviewed but not shown) and 3 h; however, this difference disappeared after overnight plating (Fig. 4A). To further investigate if dematin modulates the translocation of RhoA to the membrane, cellular fractionation assays were performed. In WT cells plated for 3 h, the RhoA translocated to the membrane and was activated. In contrast, the HPKO fibroblasts showed an approximately twofold increase of activated RhoA in the membrane fraction (Fig. 4B). Furthermore, RhoA hyperactivation in the dematin-expressing HPKO fibroblasts appears to be a conserved phenomenon, as a similar activation of RhoA was observed in the primary HPKO mouse adipocytes, as quantified by a GTPase-linked immunosorbent assay (data reviewed but not shown). These observations suggest that dematin functions as a negative regulator of RhoA activation and may participate in the activation and translocation of RhoA to the membrane compartments.

Dematin-mediated suppression of RhoA activation. RhoA activation was measured in the WT and HPKO fibroblasts transfected with the full-length, core domain, and headpiece domain constructs of dematin. WT fibroblasts transfected with the full-length dematin and headpiece domain did not show any significant reduction in RhoA activation. Interestingly, transfection of the core domain resulted in hyperactivation of RhoA (Fig. 4C). This result suggests a dominant-negative effect of the core domain in WT fibroblasts. In contrast, the HPKO fibroblasts transfected with the full-length dematin showed a significant decrease in RhoA activation (Fig. 4C). Interestingly, the transfection of HPKO cells with the headpiece and core domains did not affect RhoA activation, consistent with the morphology rescue experiments. Finally, the RNAi-induced knockdown of dematin in WT cells caused an approximately twofold increase in RhoA activation (Fig. 4D). Additionally, the knockdown of the residual core domain in HPKO fibroblasts by using siRNAs RC2 and the RC1/RC2 combination had no effect on RhoA activation. This result suggests that the activation of RhoA in HPKO fibroblasts is due to a null effect instead of the "gain-of-function" effect from the remaining core domain.

Dematin acts upstream of RhoA and FAK. To determine if RhoA hyperactivation persists in the HPKO fibroblasts upon inhibition of FAK, we used FRNK, the dominant-negative FAK-related nonkinase. WT and HPKO cells were transfected with FRNK overnight, replated for 3 h, and analyzed for RhoA activation (Fig. 5A). As expected, the WT cells transfected with FRNK showed hyperactivation of RhoA whereas the HPKO cells transfected with FRNK showed enhanced RhoA activation (Fig. 5A). This result suggests that dematin induces FAK activation through RhoA. To further substantiate this observation, the HPKO cells were treated with Rho kinase inhibitor Y27632 and then analyzed for FAK activation, as measured by FAK phosphorylation at tyrosine 397 (Fig. 5B). Inhibition of RhoA in HPKO cells caused a significant reduction in the activation of FAK. Moreover, the treatment of HPKO cells with a cell-permeable RhoA inhibitor C3-exoenzyme resulted in the rescue of the morphology defect (Fig. 5C).

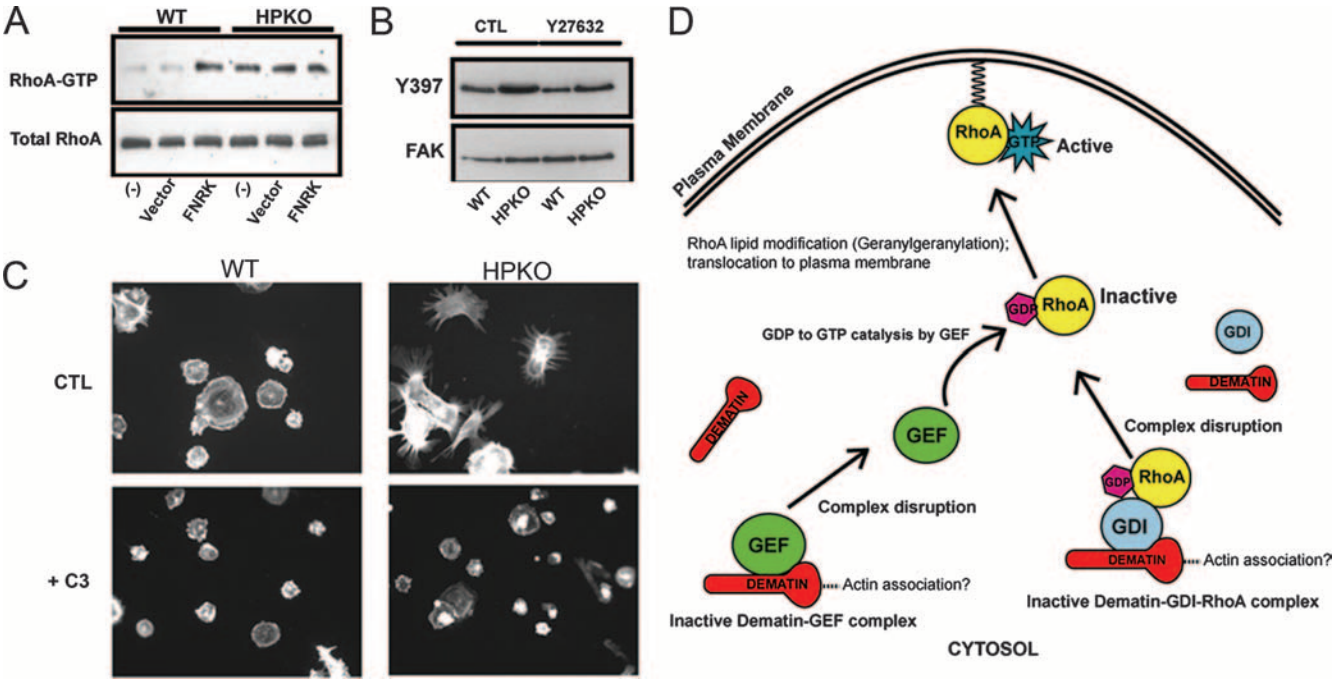

FIG. 5. Dematin regulates FAK activation through RhoA. (A) WT and HPKO (KO) MEFs transfected with an empty vector or with FRNK followed by a rhotekin-RBD pulldown assay. (B) Western blot of WT and KO MEFs treated with Y27632 and blotted for pFAKY397 and FAK as a loading control (CTL). (C) Cell morphology of WT and HPKO fibroblasts treated with C3 toxin for 1 h and replated for 3 h. Actin staining by phalloidin (red) is shown. Magnification, ×10. (D) Proposed signaling model of RhoA suppression by dematin. GEF, guanine nucleotide exchange factor.

Together, these data imply that dematin acts upstream of RhoA, resulting in the activation of FAK in the primary fibroblasts.

DISCUSSION

This paper presents the first evidence for a biological function of dematin in fibroblasts, demonstrating its critical role in cell shape changes, motility, adhesion, and wound healing pathways. Importantly, our studies unveil a hitherto-unknown function of dematin in the regulation of RhoA activation. The morphology defect observed in the HPKO fibroblasts demonstrates a functional role for dematin in the suppression of the spiky shape phenotype (Fig. 1). In WT fibroblasts, dematin is found in the perinuclear, cytoplasmic, and membrane compartments, with little overlap with actin (Fig. 1). This observation suggests that the physiological role of dematin in nonerythroid cells may be independent of its direct interaction with actin filaments. The enhanced membrane protrusions and increased stress fiber formation in the HPKO fibroblasts are features that are consistent with the activation of Rho family GTPases. The reduced motility of dematin-expressing HPKO fibroblasts was maintained with various adhesion proteins, implying that the motility defect is not influenced by the adhesive signals emanating from the extracellular matrix and is a consequence of inside-out signaling rather than the outside-in signals.

The in vitro motility defect of dematin-expressing HPKO fibroblasts translated into an in vivo wound healing defect (Fig. 3). It is unlikely that the motility defect alone can explain the highly complex wound healing phenotype, as the in vivo defect is likely to be a culmination of multiple abnormalities, including impaired fibroblast migration, collagen secretion, neovascularization, and/or leukocyte migration. The HPKO mice display a mild form of hemolytic anemia and spherocytosis. Although it is unlikely that the underlying anemia would have a significant effect on the wound healing phenotype, it is plausible that a number of factors such as the keratinocyte migration and wound reepithelialization mediated by the muscarinic receptors could contribute to the observed phenotype by intersecting with the RhoA signaling pathway (9). Alternatively, the wound healing defect could be explained by the enhanced FAK activation and increased cell adhesion of HPKO cells to the extracellular matrix proteins. FAK activation can occur via multiple signaling pathways, including adhesion-dependent integrin-mediated signaling and cues from the lysophosphatidic acid receptor (19, 20). Phosphorylated $pFAK_{Y397}$ binds to Src, resulting in stable FAK-Src complexes, thus recruiting paxillin and talin to focal adhesions (8, 26, 30). In fact, FAK activation could also activate p190RhoGAP, resulting in RhoA suppression (14). Together, a complex array of signaling events can regulate the wound healing defect observed in the dematin-expressing HPKO mice.

Among the Rho family of GTPases involved in actin cytoskeleton rearrangements, RhoA emerged as the specific target of dematin in fibroblasts. Moreover, the inhibition of FAK by dominant negative FRNK did not affect RhoA hyperactivation in the HPKO fibroblasts, and pharmacological inhibition of Rho kinase caused suppression of FAK activation (Fig. 5). These observations suggest that dematin-mediated suppression of RhoA is independent of FAK activation. Although the

precise mechanism of dematin-mediated suppression of RhoA activation is not known at present, several models could be invoked to account for RhoA suppression by dematin (Fig. 5). In principle, dematin may bind to the DH domain of a RhoA-guanine nucleotide exchange factor, thus inhibiting its activity for RhoA activation, a feature consistent with the interaction of dematin with RasGRF2 (21). Alternatively, dematin may function as a novel guanine nucleotide dissociation inhibitor (GDI) or may bind to a known GDI, akin to the binding of GDI with the cytoskeletal proteins ezrin, radixin, and moesin, which are known to regulate Rho GTPases (12, 28). In addition, dematin may also anchor the GDI-RhoA-GDP complex in the cytosol by its association with the actin filaments. The loss of the dematin headpiece would then result in the release of RhoA-GDP to interact with RhoA-guanine nucleotide exchange factor, thus converting RhoA into an active sate. It is also reasonable to speculate that the phenotypes observed in the HPKO cells are regulated by a biochemical cascade involving several steps in addition to those that we have proposed in Fig. 5. In summary, our findings provide the first evidence that dematin may function as a suppressor of RhoA activation in fibroblasts. Since homologues of dematin are found in a variety of tissues, it is likely that dematin's inhibitory activity against RhoA would be a widely conserved mechanism. The abundance of both dematin and RhoA in the erythrocyte membrane also raises the possibility that novel features of this inhibitory switch could be further delineated by applying the powerful techniques of red cell biochemistry in future studies.

ACKNOWLEDGMENTS

We are grateful to Luisa DiPietro of UIC Dental School for guidance, reagents, and analysis of the in vivo wound healing experiments. We thank John O'Bryan for suggesting the use of proteasome inhibitors in fibroblasts. We are also grateful to Dolly Mehta and Vidisha Kini for providing us guidance and reagents for the Rho GTPase and FAK assays. We thank Toshihiko Hanada and Anwar Khan for their numerous suggestions and help during the course of these studies. We are also thankful to other members of the laboratory, including Brendan Quinn, Shafi Kuchay, and Xuerong Li.

This work was supported by National Institutes of Health grant HL51445 (to A.C.).

REFERENCES

1. **Azim, A. C., A. C. Kim, M. Lutchman, S. Andrabi, L. L. Peters, and A. H. Chishti.** 1999. cDNA sequence, genomic structure, and expression of the mouse dematin gene (Epb4.9). Mamm. Genome. **10:**1026–1029.
2. **Azim, A. C., J. H. Knoll, A. H. Beggs, and A. H. Chishti.** 1995. Isoform cloning, actin binding, and chromosomal localization of human erythroid dematin, a member of the villin superfamily. J. Biol. Chem. **270:**17407–17413.
3. **Bagrodia, S., S. J. Taylor, C. L. Creasy, J. Chernoff, and R. A. Cerione.** 1995. Identification of a mouse p21Cdc42/Rac activated kinase. J. Biol. Chem. **270:**22731–22737.
4. **Barry, S. T., and D. R. Critchley.** 1994. The RhoA-dependent assembly of focal adhesions in Swiss 3T3 cells is associated with increased tyrosine phosphorylation and the recruitment of both pp125FAK and protein kinase C-delta to focal adhesions. J. Cell Sci. **107**(Pt. 7)**:**2033–2045.
5. **Bennett, V.** 1989. The spectrin-actin junction of erythrocyte membrane skeletons. Biochim. Biophys. Acta **988:**107–121.
6. **Bretscher, A., and K. Weber.** 1979. Villin: the major microfilament-associated protein of the intestinal microvillus. Proc. Natl. Acad. Sci. USA **76:**2321–2325.
7. **Chen, H., A. A. Khan, F. Liu, D. M. Gilligan, L. L. Peters, J. Messick, W. M. Haschek-Hock, X. Li, A. E. Ostafin, and A. H. Chishti.** 2007. Combined deletion of mouse dematin-headpiece and beta-adducin exerts a novel effect on the spectrin-actin junctions leading to erythrocyte fragility and hemolytic anemia. J. Biol. Chem. **282:**4124–4135.
8. **Chen, H. C., P. A. Appeddu, J. T. Parsons, J. D. Hildebrand, M. D. Schaller, and J. L. Guan.** 1995. Interaction of focal adhesion kinase with cytoskeletal protein talin. J. Biol. Chem. **270:**16995–16999.
9. **Chernyavsky, A. I., J. Arredondo, J. Wess, E. Karlsson, and S. A. Grando.** 2004. Novel signaling pathways mediating reciprocal control of keratinocyte migration and wound epithelialization through M3 and M4 muscarinic receptors. J. Cell Biol. **166:**261–272.
10. **DiPietro, L. A., M. Burdick, Q. E. Low, S. L. Kunkel, and R. M. Strieter.** 1998. MIP-1α as a critical macrophage chemoattractant in murine wound repair. J. Clin. Investig. **101:**1693–1698.
11. **Hall, A.** 2005. Rho GTPases and the control of cell behaviour. Biochem. Soc. Trans. **33:**891–895.
12. **Hirao, M., N. Sato, T. Kondo, S. Yonemura, M. Monden, T. Sasaki, Y. Takai, and S. Tsukita.** 1996. Regulation mechanism of ERM (ezrin/radixin/moesin) protein/plasma membrane association: possible involvement of phosphatidylinositol turnover and Rho-dependent signaling pathway. J. Cell Biol. **135:**37–51.
13. **Hocking, D. C., J. Sottile, and P. J. McKeown-Longo.** 1998. Activation of distinct α5β1-mediated signaling pathways by fibronectin's cell adhesion and matrix assembly domains. J. Cell Biol. **141:**241–253.
14. **Holinstat, M., N. Knezevic, M. Broman, A. M. Samarel, A. B. Malik, and D. Mehta.** 2006. Suppression of RhoA activity by focal adhesion kinase-induced activation of p190RhoGAP: role in regulation of endothelial permeability. J. Biol. Chem. **281:**2296–2305.
15. **Husain-Chishti, A., W. Faquin, C. C. Wu, and D. Branton.** 1989. Purification of erythrocyte dematin (protein 4.9) reveals an endogenous protein kinase that modulates actin-bundling activity. J. Biol. Chem. **264:**8985–8991.
16. **Husain-Chishti, A., A. Levin, and D. Branton.** 1988. Abolition of actin-bundling by phosphorylation of human erythrocyte protein 4.9. Nature **334:**718–721.
17. **Khanna, R., S. H. Chang, S. Andrabi, M. Azam, A. Kim, A. Rivera, C. Brugnara, P. S. Low, S. C. Liu, and A. H. Chishti.** 2002. Headpiece domain of dematin is required for the stability of the erythrocyte membrane. Proc. Natl. Acad. Sci. USA **99:**6637–6642.
18. **Kumagai, N., N. Morii, K. Fujisawa, Y. Nemoto, and S. Narumiya.** 1993. ADP-ribosylation of rho p21 inhibits lysophosphatidic acid-induced protein tyrosine phosphorylation and phosphatidylinositol 3-kinase activation in cultured Swiss 3T3 cells. J. Biol. Chem. **268:**24535–24538.
19. **Kumagai, N., N. Morii, K. Fujisawa, T. Yoshimasa, K. Nakao, and S. Narumiya.** 1993. Lysophosphatidic acid induces tyrosine phosphorylation and activation of MAP-kinase and focal adhesion kinase in cultured Swiss 3T3 cells. FEBS Lett. **329:**273–276.
20. **Lipfert, L., B. Haimovich, M. D. Schaller, B. S. Cobb, J. T. Parsons, and J. S. Brugge.** 1992. Integrin-dependent phosphorylation and activation of the protein tyrosine kinase pp125FAK in platelets. J. Cell Biol. **119:**905–912.
21. **Lutchman, M., A. C. Kim, L. Cheng, I. P. Whitehead, S. S. Oh, M. Hanspal, A. A. Boukharov, T. Hanada, and A. H. Chishti.** 2002. Dematin interacts with the Ras-guanine nucleotide exchange factor Ras-GRF2 and modulates mitogen-activated protein kinase pathways. Eur. J. Biochem. **269:**638–649.
22. **Lutchman, M., S. Pack, A. C. Kim, A. Azim, M. Emmert-Buck, C. van Huffel, Z. Zhuang, and A. H. Chishti.** 1999. Loss of heterozygosity on 8p in prostate cancer implicates a role for dematin in tumor progression. Cancer Genet. Cytogenet. **115:**65–69.
23. **Rana, A. P., P. Ruff, G. J. Maalouf, D. W. Speicher, and A. H. Chishti.** 1993. Cloning of human erythroid dematin reveals another member of the villin family. Proc. Natl. Acad. Sci. USA **90:**6651–6655.
24. **Ren, X. D., W. B. Kiosses, and M. A. Schwartz.** 1999. Regulation of the small GTP-binding protein Rho by cell adhesion and the cytoskeleton. EMBO J. **18:**578–585.
25. **Rogers, S., R. Wells, and M. Rechsteiner.** 1986. Amino acid sequences common to rapidly degraded proteins: the PEST hypothesis. Science **234:**364–368.
26. **Schaller, M. D., C. A. Otey, J. D. Hildebrand, and J. T. Parsons.** 1995. Focal adhesion kinase and paxillin bind to peptides mimicking beta integrin cytoplasmic domains. J. Cell Biol. **130:**1181–1187.
27. **Siegel, D. L., and D. Branton.** 1985. Partial purification and characterization of an actin-bundling protein, band 4.9, from human erythrocytes. J. Cell Biol. **100:**775–785.
28. **Takahashi, K., T. Sasaki, A. Mammoto, K. Takaishi, T. Kameyama, S. Tsukita, and Y. Takai.** 1997. Direct interaction of the Rho GDP dissociation inhibitor with ezrin/radixin/moesin initiates the activation of the Rho small G protein. J. Biol. Chem. **272:**23371–23375.
29. **Watanabe, N., T. Kato, A. Fujita, T. Ishizaki, and S. Narumiya.** 1999. Cooperation between mDia1 and ROCK in Rho-induced actin reorganization. Nat. Cell Biol. **1:**136–143.
30. **Xing, Z., H. C. Chen, J. K. Nowlen, S. J. Taylor, D. Shalloway, and J. L. Guan.** 1994. Direct interaction of v-Src with the focal adhesion kinase mediated by the Src SH2 domain. Mol. Biol. Cell **5:**413–421.